ACIS Sub-Pixel Resolution: Improvement in Point Source Detection

Craig S. Anderson,[1] Amy E. Mossman,[1] Dong-Woo Kim,[1] Glenn E. Allen,[2]
Kenny J. Glotfelty,[1] and Giuseppina Fabbiano[1]

[1]*Smithsonian Astrophysical Observatory, 60 Garden Street, Cambridge, MA 02138, USA*

[2]*MIT Kavli Institute for Astrophysics and Space Research, 77 Massachusetts Avenue, 37-287, Cambridge, MA 02139*

Abstract.   We investigate how to achieve the best possible ACIS spatial resolution by binning in ACIS sub-pixel and applying an event repositioning algorithm after removing pixel-randomization from the pipeline data. We quantitatively assess the improvement in spatial resolution by (1) measuring point source sizes and (2) detecting faint point sources. The size of a bright (but no pile-up), on-axis point source can be reduced by 20–30%. With the improved resolution, we detect ∼ 20% more faint sources when embedded in the extended, diffuse emission in a crowded field. We further discuss the false source rate of ∼ 10% among the newly detected sources, using a few ultra-deep observations.

1.   How to Obtain the Best Possible ACIS Resolution

In order to achieve the best possible ACIS resolution, we apply the following steps to the Chandra X-ray Center (CXC) pipeline products. Then we quantitatively assess the improvement by comparing the point source sizes (§ 2) and detections (§ 3) before and after the procedure.

Sub-pixel binning: Chandra coordinates contain positional accuracy finer than one ACIS pixel (0.492 arcsec) through dither and aspect correction. Imaging data binned by ACIS sub-pixel can already provide an improved resolution.

Remove pixel randomization: The current pipeline default is to apply pixel randomization by 1/2 ACIS pixel on the chip coordinate to remove the instrumental "gridded" appearance of the data and to avoid any possible aliasing affects associated with this spatial grid. This pixel randomization has to be removed before applying a sub-pixel algorithm.

ACIS sub-pixel algorithm: Positional accuracy can be improved by utilizing the positional information in 3×3 event islands. Several sub-pixel event repositioning algorithms have been developed during the first years of the Chandra mission. The first implementation by Tsunemi et al. (2001) applied the knowledge of charge cloud size in 3×3 event islands to corner events with ASCA grade 6 (4–16% of on-axis events). Mori et al. (2001) extended the algorithm to all split pixel events: event grades 2, 3, 4 are shifted 1/2 pixel in one direction, grade 6 events are shifted 1/2 pixel in two directions, while grade 0 events remain centered on the event island. Later Li et al. (2003, 2004) improved the algorithm to SER (subpixel event repositioning) and further to EDSER (energy dependent SER). CXC also implemented EDSER[1] in CIAO 4.3.[2]

PSF deconvolution: We do not discuss deconvolution here. We refer the reader to CXC Announcement #64.[3]

---

[1]`http://space.mit.edu/CXC/docs/docs.html#subpix`

[2]`http://cxc.harvard.edu/ciao/releasenotes/ciao_4.3_release.html`

[3]`http://cxc.harvard.edu/announcements/announce_64.html`
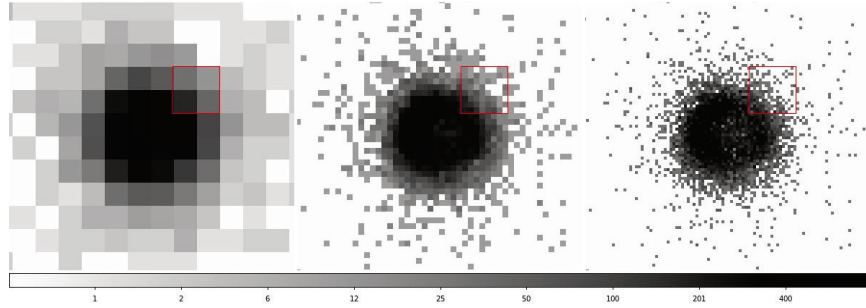
Figure 1.   SN1987A (Energy 300–5000eV)
The improved resolution is shown for a bright extended source with binning of 1, 1/4, and 1/8 pixel (left to right). Images have pixel randomization removed and a sub-pixel event repositioning algorithm applied. Red squares are 1 arcsecond per side. See also Park et al. (2002).

2.   Testing Improvement of Point Source Sizes

We selected seven bright sources (5 on-axis, 2 off-axis) with pile-up fraction less than 5%. Source sizes presented in Table 1 were measured by the CIAO tool srcextent[4] which calculates the size (sigma) and associated uncertainty of a photon-count source image using the Mexican Hat Optimization algorithm (Houck 2007). The uncertainty (at 90% confidence) is derived from Monte Carlo trials. Applying sub-pixel binning of 1/4 pixel reduces the on-axis source size by 19–24%. Additionally removing pixel randomizaton and applying the sub-pixel event repositioning algorithm further reduces the on-axis source size by another 6–8%. Off-axis sources show no statistical improvement.

3.   Testing Improvement of Faint Source Detections Embedded in Diffuse Emission

With the improved resolution, we present in Table 2 ~20% more faint source detections embedded in extended, diffuse emission in a crowded field. To check whether the new sources are real or suprious, we compare sources detected in shallow and deep images. We assume that the real sources which are newly found in the shallow image will be detected in the deep image. We also find an increase of ~10% in false source detections defined as those newly found in the shallow image, but not in the deep image. Because some point sources (LMXBs) in elliptical galaxies are variable, the false source rate is actually an upper limit. To lessen the effect of variable sources, we cut a deep observation (90–110 ks) into smaller pieces (10ks and 20ks), instead of merging multiple observations with months or years between exposures.

After sub-pixel binning by 1/2 pixel the fraction of newly detected sources is ~9% (21/240, 38/306) of which 12–14% (3/21, 3/28) may be false. Binning by 1/2 pixel and applying the SER algorithm the fraction of new sources is 15–28% (36/240, 86/306) of which 3–8% (3/36, 3/86) may be false. However, 8–10% (15/240, 31/306) of the original sources (6–20% of them may be false) detected in the pipeline product are lost, indicating that the original detections are still needed. We find no improvement when the background and diffuse emissions are low, e.g., Chandra Deep Field.

---

[4]`http://cxc.harvard.edu/ciao/ahelp/srcextent.html`

Figure 2. Example of additional faint source detections.
Source regions output by wavdetect tool on ACIS image data after removal of pixel randomization, sub-pixel binning, and SER algorithm applied.

Table 1. Point Source Size Improvement

ObsID	pipeline products		pixel randomization off		sub-pixel algorithm applied			
			binning by 1 pixel					
02228	0.51	(0.47-0.54)	0.48	(0.44-0.53)	0.47	(0.43-0.52)		
02254	0.73	(0.69-0.76)	0.72	(0.68-0.75)	0.71	(0.68-0.75)		
00927	0.63	(0.60-0.66)	0.62	(0.59-0.64)	0.62	(0.59-0.64)		
01602	0.76	(0.71-0.81)	0.74	(0.69-0.79)	0.72	(0.67-0.77)		
03140	0.57	(0.51-0.62)	0.55	(0.50-0.60)	0.56	(0.51-0.61)		
04964	1.75	(1.66-1.83)	1.75	(1.67-1.84)	1.75	(1.66-1.84)		
04936	1.02	(0.98-1.05)	1.00	(0.97-1.04)	1.00	(0.96-1.03)		
			binning by 1/2 pixel				improvement(%)	
02228	0.44	(0.40-0.47)	0.41	(0.38-0.44)	0.40	(0.37-0.43)	14	22
02254	0.62	(0.59-0.65)	0.60	(0.57-0.63)	0.59	(0.56-0.63)	15	19
00927	0.50	(0.48-0.52)	0.49	(0.46-0.51)	0.48	(0.46-0.51)	21	24
01602	0.61	(0.57-0.65)	0.59	(0.55-0.64)	0.58	(0.54-0.62)	20	24
03140	0.44	(0.40-0.47)	0.41	(0.38-0.45)	0.38	(0.35-0.41)	23	33
04964	1.74	(1.65-1.82)	1.73	(1.65-1.82)	1.73	(1.65-1.82)	1	1
04936	1.00	(0.97-1.04)	0.98	(0.95-1.02)	0.98	(0.94-1.02)	2	4
			binning by 1/4 pixel				improvement(%)	
02228	0.43	(0.40-0.46)	0.40	(0.37-0.43)	0.39	(0.37-0.42)	16	24
02254	0.57	(0.54-0.60)	0.56	(0.54-0.59)	0.56	(0.54-0.59)	22	23
00927	0.45	(0.43-0.47)	0.43	(0.41-0.45)	0.42	(0.40-0.44)	29	33
01602	0.59	(0.56-0.63)	0.54	(0.51-0.57)	0.51	(0.48-0.55)	22	33
03140	0.39	(0.36-0.43)	0.40	(0.37-0.43)	0.30	(0.28-0.33)	32	47
04964	1.74	(1.66-1.83)	1.73	(1.65-1.82)	1.74	(1.65-1.82)	1	1
04936	1.03	(0.99-1.06)	0.99	(0.95-1.02)	0.98	(0.95-1.02)	0	4

Sources for ObsID's 04964,04936 are off-axis

Table 2.   Source Detection Comparison

		O	sub-pixel binning				binning + sub-pixel algorithm			
			A	B	C	D	A	B	C	D
			NGC 3379 obsid=7073 (87 ks)							
1	10ks	32	2-0	4-0	2-0	4-0	2-0	11-2	2-0	9-0
2	10ks	34	2-0	4-1	2-0	2-0	2-1	3-0	2-1	3-0
3	10ks	30	0-0	2-0	0-0	2-0	0-0	2-1	0-0	2-0
4	20ks	52	2-0	4-3	2-0	3-2	4-1	9-6	4-0	7-2
5	20ks	48	1-0	3-4	1-0	2-0	1-1	6-1	1-1	5-0
6	20ks	44	2-2	6-4	2-2	5-1	3-1	7-2	3-1	7-1
Subtotal		240	9-2	23-12	9-2	18-3	12-4	38-12	12-3	33-3
			NGC 4278 obsid=7081 (114 ks)							
1	10ks	40	2-0	8-1	1-0	3-1	5-0	16-1	5-0	9-1
2	10ks	40	5-0	7-0	5-0	6-0	6-1	17-1	6-1	13-1
3	10ks	38	3-0	3-2	2-0	1-1	3-0	15-0	3-0	8-0
4	20ks	62	1-0	14-5	1-0	10-0	3-0	20-11	3-0	14-1
5	20ks	61	6-0	9-5	6-0	4-1	6-0	26-3	6-0	22-0
6	20ks	65	2-1	3-2	2-1	1-1	6-1	19-7	6-1	17-0
Subtotal		306	19-1	44-15	17-1	25-3	29-2	113-23	29-2	83-3
Total		546	28-3	67-27	26-3	43-6	41-6	151-35	41-5	126-6

For n-m; n,(m) = number of new sources (not) confirmed in deeper image
O. number of sources from the pipeline image binned by ACIS pixel (0.492")
A. number of lost sources (i.e., detected in the raw image, but not in the sub-pix image)
B. number of new sources (i.e., detected in the sub-pix image, but not in the raw image)
C, D. same as A, B but excludes those sources with 0 size by wavdetect (r_major=r_minor=0)

References

Houck, J. C. 2007, Measuring Detected Source Extent Using Mexican-Hat Optimization, Tech. rep., MIT Kavli Institute for Astrophysics and Space Science. URL `http://cxc.cfa.harvard.edu/csc/memos/files/Houck_source_extent.pdf`

Li, J., Kastner, J. H., Prigozhin, G. Y., & Schulz, N. S. 2003, ApJ, 590, 586

Li, J., Kastner, J. H., Prigozhin, G. Y., Schulz, N. S., Feigelson, E. D., & Getman, K. V. 2004, ApJ, 610, 1204

Mori, K., Tsunemi, H., Miyata, E., Baluta, C. J., Burrows, D. N., Garmire, G. P., & Chartas, G. 2001, in New Century of X-ray Astronomy, edited by H. Inoue & H. Kunieda (San Francisco, CA: ASP), vol. 251 of ASP Conf. Ser., 576

Park, S., Burrows, D. N., Garmire, G. P., Nousek, J. A., McCray, R., Michael, E., & Zhekov, S. 2002, ApJ, 567, 314

Tsunemi, H., Mori, K., Miyata, E., Baluta, C., Burrows, D. N., Garmire, G. P., & Chartas, G. 2001, ApJ, 554, 496